

RESEARCH ARTICLE

Thin Al₂O₃ passivated boron emitter of n-type bifacial c-Si solar cells with industrial process

Guilin Lu¹, Fei Zheng², Jianqiang Wang² and Wenzhong Shen^{1,3*}

¹ Institute of Solar Energy, and Key Laboratory of Artificial Structures and Quantum Control (Ministry of Education), Department of Physics and Astronomy, Shanghai Jiao Tong University, Shanghai 200240, China

² Shanghai Shenzhou New Energy Development Co., Ltd., Shanghai 201112, China

³ Collaborative Innovation Center of Advanced Microstructures, Nanjing 210093, China

ABSTRACT

We have presented thin Al₂O₃ (~4 nm) with SiN_x:H capped (~75 nm) films to effectively passivate the boron-doped p⁺ emitter surfaces of the n-type bifacial c-Si solar cells with BBr₃ diffusion emitter and phosphorus ion-implanted back surface field. The thin Al₂O₃ capped with SiN_x:H structure not only possesses the excellent field effect and chemical passivation, but also establishes a simple cell structure fully compatible with the existing production lines and processes for the low-cost n-type bifacial c-Si solar cell industrialization. We have successfully achieved the large area (238.95 cm²) high efficiency of 20.89% (front) and 18.45% (rear) n-type bifacial c-Si solar cells by optimizing the peak sintering temperature and fine finger double printing technology. We have further shown that the conversion efficiency of the n-type bifacial c-Si solar cells can be improved to be over 21.3% by taking a reasonable high emitter sheet resistance. Copyright © 2017 John Wiley & Sons, Ltd.

KEYWORDS

c-Si solar cells; n-type bifacial; thin Al₂O₃; industrial process

*Correspondence

Wenzhong Shen, Institute of Solar Energy, and Key Laboratory of Artificial Structures and Quantum Control (Ministry of Education), Department of Physics and Astronomy, Shanghai Jiao Tong University, Shanghai 200240, China.

E-mail: wzshen@sjtu.edu.cn

Received 3 October 2015; Revised 5 December 2016; Accepted 8 December 2016

1. INTRODUCTION

N-type crystalline Si (c-Si) solar cells have been proven to have a higher tolerance to common impurities (e.g., Fe) [1] and do not suffer from the boron–oxygen related light-induced degradation [2], which is known to be the problem for p-type Si counterparts. Recently, n-type bifacial c-Si solar cells receive a great attention due to the symmetric configuration in which sunlight is harnessed from both front and rear sides [3], leading to the significant advantage on energy outputs over the conventional front surface field solar cells. The n-Pasha cell from ECN is a typical bifacial solar cell with average efficiencies between 19.8% and 20.0% [4], where the p⁺ boron (B) emitter and n⁺ phosphorus (P) back surface field (BSF) are formed with thermal diffusion using the tube furnace after double-side texturing. The two different and appropriate diffusion profiles (p⁺ emitter and n⁺ BSF) were generated by varying the diffusion temperature

and time to realize the different sheet resistances and junction depths. Very recently, they have achieved a high cell efficiency of 20.7% in combination with the selective emitter technology [5].

One of the great challenges of this bifacial structure cells (p⁺–n–n⁺) lies in passivating p⁺ emitters effectively. Agostinelli *et al.* [6] demonstrated a degradation of minority carrier lifetime for n-type wafers with B-doped surfaces passivated with SiO₂/SiN_x:H under thermal or light aging. Gatz *et al.* [7] obtained a high-quality passivation on p-type surfaces with a-Si:H/SiN_x stacks at temperature below 400 °C, but suffered from insufficient thermal stability after 30-min annealing at 500 °C. Recently, a very effective passivation of p-type surfaces by Al₂O₃ (10–30 nm) deposited by plasma-assisted atomic layer deposition (ALD) has been demonstrated [8–11]. The excellent passivation stability of the Al₂O₃ and Al₂O₃/SiN_x:H stacks under thermal and light soaking condition has also been proved by Dingemans *et al.* [12] The state-of-the-art

surface passivation properties of Al₂O₃ are attributed to a reasonable chemical surface passivation with a rather low density defects D_{it} ($\sim 10^{11} \text{ eV}^{-1} \text{ cm}^{-2}$) and a strong field effect passivation due to a high density of fixed negative charges Q_f (10^{12} – 10^{13} cm^{-2}) located near the Si surfaces [13–15]. Especially, the built-in negative electric field provided by Al₂O₃ causes a reduction of the electron density (the minority carriers) of the p-type Si surfaces [16]. Some researchers have further deduced that the negative Q_f is located at the internal dielectric between the SiO₂ interface layer and the Al₂O₃ layer [17–19], and Werner *et al.* [20] demonstrated that both the high Q_f and D_{it} decreased from 1 to 5 nm thickness for the Al₂O₃ samples, while the variation trend was not obvious from 5 to 31 nm thickness. However, previous relevant Al₂O₃ capped with SiN_x:H studies of surface passivation and antireflection coating layer have been only on n-type single-sided Si solar cells [21].

In this work, we have proposed thin Al₂O₃ (up to 5 nm) with SiN_x:H capped (75 nm) films to passivate the B-doped p⁺ emitter surfaces. Al₂O₃ with a wealth of negative charge mainly serves for the role of the field effect passivation, and the chemical passivation is mostly provided by the SiN_x:H capping layer. We have achieved the high efficiency of 20.89% n-type bifacial c-Si solar cells (238.95 cm²) using boron tribromide (BBr₃) diffusion emitter and P ion-implanted BSF (to realize the front and back side doping easily and steadily, rather than the conventional complicated bifacial diffusion or co-diffusion) in conjunction with screen printed contacts. We have used a co-firing step to sinter the different metallization pastes and to form electrical contacts for the front p⁺ emitter and rear n⁺ BSF, i.e., there is no need to open the front side dielectric passivation layer with laser or etching pastes due

to the thin Al₂O₃. The present thin Al₂O₃ layer and its composite SiN_x:H structure, together with the simplified process from the traditional n-Pasha cell structure, have great advantages in the process of n-type bifacial c-Si solar cell industrialization, not only passivating the p⁺ emitter surfaces effectively, but also compatible with the current industrial process at a low cost.

2. EXPERIMENTAL AND SIMULATION DETAILS

2.1. Fabrication of n-type bifacial solar cells

Figure 1 shows the schematic structure used in this study to demonstrate the applicability of thin Al₂O₃ front surface p⁺ emitter passivation to high-efficiency n-type bifacial c-Si solar cells. As starting material, we used (100)-oriented n-type Cz wafers (238.95 cm²) with a thickness of 180 μm and a resistivity of 3–4 Ω cm. After damage etching of ~10 μm/side, alkaline texturing and RCA clean, all the samples were diffused back to back via a conventional BBr₃ (E2000 HT 300-5, Centrotherm, Germany), where the inner side would not be effectively diffused as the outside of the wafers. Afterwards, the edge isolation and rear side were polished using a mixture of hydrofluoric acid and nitric acid solution, and the boronsilicate glass layer was removed in diluted hydrofluoric acid solution (5% by volume) allowing the detailed emitter characterization, resulting in a p⁺ emitter with a sheet resistance of 57 Ω/□. After the chemical etching, P ions were implanted with an acceleration voltage of 15 keV and a dose of $3.2 \times 10^{15} \text{ cm}^{-2}$ on the quasi-planar rear side (IonSolarTM, Kingstonesemi, China). The

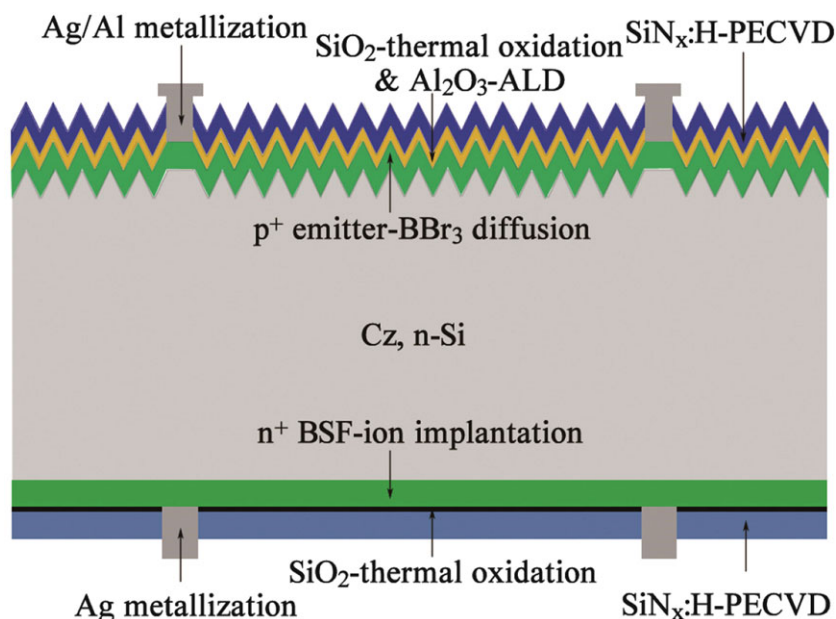


Figure 1. Schematic structure of n-type random pyramid textured front B diffusion p⁺ emitter and quasi-planar rear P ion-implantation n⁺ BSF bifacial c-Si solar cells. [Colour figure can be viewed at wileyonlinelibrary.com]

annealing temperature of P implanted n⁺ BSF is not just like the B implanted p⁺ emitter with a high temperature (>1000 °C) and long time to create deep junctions [22]. We had employed a low temperature (800 °C, 30 min) activation annealing and oxidation, resulting in ~1.5–2.0 nm SiO₂ on the p⁺ emitter and n⁺ BSF, together with a sheet resistance of p⁺ emitter increasing from 57 to 63 Ω/□ and an n⁺ BSF of 37 Ω/□. Different thicknesses (0, 2, 3, 4, and 5 nm) of Al₂O₃ were then deposited by ALD (TFS 200, Beneq, Finland) at 185 °C on the p⁺ emitter surfaces, capped by SiN_x:H (fixed thickness of 75 nm) films by plasma enhanced chemical vapor deposition (PECVD) (SINA XS, Roth & Rau, Germany) on both sides of the wafers. The fixed charge density in the Al₂O₃/p⁺ emitter combined structure has been calculated to be $-3.65 \times 10^{12} \text{ cm}^{-2}$ with the help of the measured flat band voltage of 2.587 V from Corona charge-voltage property (PV-2000, Semilab, Hungary). Finally, contacts were ensured by the screen-printed (LTCC, Baccini, Italy) of grids using Ag/Al and Ag pastes on the front and rear sides, respectively, with a co-firing in an infra-red belt-furnace (CFD-9024, Dispatch, USA).

2.2. Simulation by EDNA2 and PC1D

To further understand the p⁺ emitter surface passivation performance of the n-type c-Si solar cell precursors, we

use the computer simulation package EDNA2 [23,24] to perform detailed p⁺ emitter saturation current density J_{0e} simulation based on four basic types of recombination: radiative, Auger, Shockley–Read–Hall, and surface recombination. In our simulation, we have employed the dopant ionization model of Altermatt *et al.*, [25] the Auger parameterization of Richter *et al.*, [26] and the Fermi–Dirac statistics together with the band gap narrowing model of Schenk [27]. We emphasize further that the input parameters are from the experimental data, including the 3.5 Ω cm n-type bulk resistivity, an industrially feasible wafer thickness of 180 μm, a sheet resistance $R_{sh}=63.1 \text{ Ω/□}$, and the peak substitutional dopant concentration $N_{peak}=9.38 \times 10^{19} \text{ cm}^{-3}$ at 0.1043 μm of the B doped p⁺ emitter surface. In addition, we also employed the PC1D software to predict the conversion efficiency of the n-type bifacial Si solar cells varying with the p⁺ emitter peak doping level from 9.38×10^{18} to $9.38 \times 10^{20} \text{ cm}^{-3}$ at different bulk resistivities (1.5–5.5 Ω cm). Table I lists the main input parameter values in the EDNA2 and PC1D simulations.

2.3. Characterization

We investigated the effect of Al₂O₃ thickness, sintering temperature, and front side finger width on the performance of these n-type bifacial c-Si solar cells. The doping profiles were measured by electrochemical capacitance–

Table I. The main input parameter values for the EDNA2 and PC1D simulations.

EDNA2-parameters	Unit	Value	PC1D-parameters	Unit	Value
Background dopant Concentration N_b	cm^{-3}	Phosphorus 1.32×10^{15}	Device area	cm^2	238.95
Resistivity ρ_b	Ω cm	3.5	Wafer thickness	μm	180
Temperature	K	300	Resistivity	Ω cm	3.5 (1.5, 2.5, 3.5, 4.5, 5.5)
Specified voltage $V_{i \text{ spec}}$	V	0.7	Front side texture depth	μm	3.535
Emitter dopant		Boron	R_{series}	Ω cm^2	0.6
Profile		Generated	R_{shunt}	Ω cm^2	5790
Sheet resistance ρ_{sheet}	Ω/sq	63.1	Metal contact coverage front/back		~6%/~4%
Function		Gaussian	τ_{bulk}	μs	1500
N_{peak}	cm^{-3}	9.38×10^{19}	FSRV	cm/s	2000
z_{peak}	μm	0.1043	BSRV	cm/s	200
z_i	μm	0.1315	Diffusion front/back		p-type (boron)/n-type (phosphorus)
Recombination and band gap models:			Profile		Gaussian
Radiative		Trupke2003 fit	First diffusion peak	cm^{-3}	9.38×10^{19}
Auger		Richter2012	doping front/back		$(9.38 \times 10^{18} - 9.38 \times 10^{20}) / 2.19 \times 10^{20}$
SRV S_{eff}	cm/s	1×10^4	Sheet resistance front/back	Ω/sq	63(8.4–362.3)/37
Dopant ionization		Altermatt2006	Junction depth front/back (3.5 Ω cm)	μm	0.62/0.85
Carrier statistics		Fermi–Dirac	Modeled Eff (3.5 Ω cm)	%	20.90
Band gap narrowing		Schenk1998	Experimental Eff (3.5 Ω cm)	%	20.89

voltage (ECV) profiling (CVP21, WEP, Germany), and the sheet resistance R_{sh} of the wafers were obtained by four-point probes (280I Series, Four Dimensions Inc., USA). The thickness and refractive index of Al₂O₃ and SiN_x:H thin films were determined by spectroscopic ellipsometry (SE400, Sentech, Germany). The implied V_{oc} and effective minority carrier lifetime τ_{eff} were obtained by quasi-steady-state photoconductance (QSSPC) method (WCT-120, Sinton Instruments, USA). The external quantum efficiency (EQE) was measured on the platform of quantum efficiency measurement (QEX10, PV Measurements, USA). The electrical parameters (open-circuit voltage V_{oc} , short-circuit current density J_{sc} , fill factor FF , and energy conversion efficiency Eff) of the solar cells were analyzed by current density–voltage (J – V) measurement under the illumination of AM1.5 with the h.a.l.m. (h.a.l.m. elektronik GmbH, Germany).

3. RESULTS AND DISCUSSION

3.1. Characteristics of solar cell precursors

Figure 2(a) presents the wafer ECV dopant profiles of the p⁺ emitter and n⁺ BSF. The p⁺ diffused emitter exhibits a surface concentration of $\sim 7.23 \times 10^{19} \text{ cm}^{-3}$ with a junction depth of 0.56 μm . After low temperature (800 °C, 30 min) activation annealing and oxidation, the P ion-implanted

yields a deep n⁺ BSF of 0.85 μm with the sheet resistance $R_{sh} = 37 \Omega/\square$ and a high surface concentration of $\sim 2.19 \times 10^{20} \text{ cm}^{-3}$. A relatively low surface concentration ($\sim 2.31 \times 10^{19} \text{ cm}^{-3}$) and deep junction depth (0.62 μm) of the p⁺ emitter were formed after the annealing process, with the sheet resistance increased from 57 to 63 Ω/\square accordingly. The annealing oxidation step resulted in deeper diffusion of B into Si and also its diffusion into the SiO₂ due to higher solid solubility and diffusion coefficient of B in SiO₂ [26]. This led to a decrease of the B surface doping concentration and thus higher sheet resistance and deeper junction depth of the p⁺ emitter.

In order to evaluate the quality of the different passivation processes, we could measure the implied V_{oc} and effective minority carrier lifetime τ_{eff} of n-type bifacial c-Si solar cells' precursors (non-metallization) [28]. The precursor structure has the characteristics of BBr₃ diffusion emitter on the textured front side and P ion-implanted BSF on the polished rear side, together with SiN_x:H/Al₂O₃/SiO₂ stack passivated front surface and SiO₂/SiN_x:H stack passivated rear surface, respectively. Figure 2(b) and 2(c) presents with different thicknesses of Al₂O₃ and fixed thickness of 75 nm SiN_x:H capped films before and after the conventional peak sintering temperature ($\sim 905 \text{ °C}$, 30 s). Obviously, the passivation quality without Al₂O₃ (0 nm group) was worse than that of other groups (2, 3, 4, and 5 nm Al₂O₃) no matter whether prior to or after sintering. This demonstrates that the passivation quality

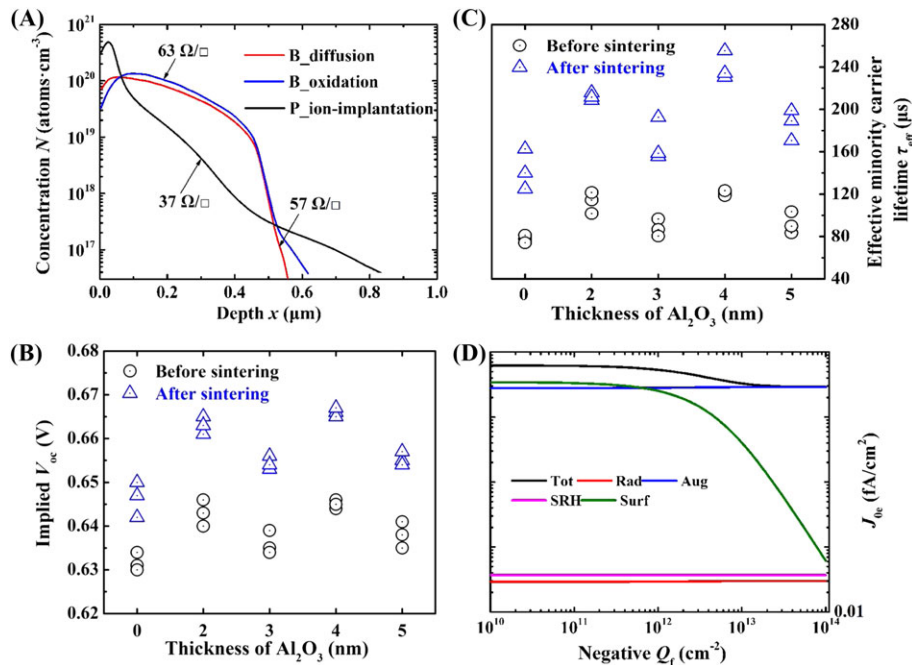


Figure 2. (a) ECV dopant profiles of the p⁺ emitter (diffusion, annealing and oxidation) and n⁺ BSF (annealing and oxidation). Passivation quality with (b) implied V_{oc} (V) and (c) effective minority carrier lifetime τ_{eff} (μs) of the different thicknesses Al₂O₃ deposited by ALD on the p⁺ emitter with fixed thickness (75 nm) bifacial SiN_x:H capped films by PECVD before and after sintering at 905 °C (30 s). (d) Modeled emitter saturation current density J_{0e} varies with the density of fixed negative charges Q_f of the p⁺ emitter surface. Types of recombination: Tot—total recombination, Rad—radiative recombination, Aug—Auger recombination, SRH—Shockley–Read–Hall recombination, and Surf—Surface recombination. [Colour figure can be viewed at wileyonlinelibrary.com]

was attributed to a reasonable chemical surface passivation and a strong field effect passivation on the p⁺ emitter Si surfaces. After sintering, the implied V_{oc} of the 2 and 4 nm Al₂O₃ groups increased from 0.645 V to above 0.660 V, accompanied with the effective minority carrier lifetime τ_{eff} reached more than 200 μ s. The increased implied V_{oc} and τ_{eff} can be attributed to the hydrogenation effect of SiO₂/Al₂O₃/SiN_x:H during the thermal treatment. The hydrogen from silicon nitride layers diffuses into the SiO₂/bulk Si interface, reducing the density of interface traps like dangling bonds and implicitly making recombinative traps inactive [29,30]. In addition, we have further yielded the emitter saturation current density J_{0e} of the symmetrically processed p⁺-n-p⁺ lifetime samples (capped with Al₂O₃ and SiN_x:H) according to the high-injection method proposed by Kane and Swanson. The experimental J_{0e} s are 104.5, 50.38, 60.20, 31.25, and 60.80 fA/cm² for the solar cells capped with 0, 2, 3, 4, and 5 nm of Al₂O₃ and fixed thickness of 75 nm SiN_x stack passivation, respectively. Obviously, the 2 and 4 nm Al₂O₃ groups have shown an excellent passivation performance on the p⁺ emitter surface of the n-type c-Si. The passivation effect in the Al₂O₃ thickness range 1–5 nm depends on the trade-off between the field effect (high fixed negative charge density Q_f) and chemical passivation (low interface state density D_{it}) [20]. We directly examined the passivation performances of five different Al₂O₃ thicknesses (0, 2, 3, 4, 5 nm). From the experimental data (implied V_{oc} , τ_{eff} , and J_{0e}), we observed that the 2 and 4 nm Al₂O₃ groups are slightly better than the 3 and 4 nm Al₂O₃ ones, as this could be due to the tiny differences between the blistering of the Al₂O₃ passivation layers [31]. This is the reason that we selected the 2 and 4 nm Al₂O₃ to passivate the p⁺ emitter of the n-type bifacial c-Si solar cells in the subsequent experiments.

3.2. Simulation of the emitter saturation current density J_{0e} of the p⁺ emitter surface

Figure 2(d) shows the simulated p⁺ emitter saturation current density J_{0e} . An increase of fixed negative charges Q_f from around 10¹² to 10¹³ cm⁻² sharply reduces the J_{0e} , where the surface recombination plays a leading role in all the recombination. The theoretical results in Figure 2 (d) demonstrate that the fixed negative charges Q_f provides a strong field effect passivation near the p⁺ emitter surface. This is consistent with the observation in Figure 2(b) and 2(c) that Al₂O₃ with high density of fixed negative charges effectively passivates the p⁺ emitter surface.

The n-type bifacial c-Si solar cell's precursor (non-metallization) is an asymmetrical structure (p⁺-n-n⁺), and the measured τ_{eff} (QSSPC method in Figure 2(c)) is closely link to the front side emitter saturation current density ($J_{0\ front}$) and back side field saturation current density ($J_{0\ back}$):

$$\frac{1}{\tau_{eff}} = \frac{1}{\tau_{bulk}} + \frac{J_{0\ front}(N_d + \Delta n)}{qn_i^2 W} + \frac{J_{0\ back}(N_d + \Delta n)}{qn_i^2 W} \quad (1)$$

As we know, τ_{eff} can be expressed by

$$\frac{1}{\tau_{eff}} = \frac{1}{\tau_{Rad}} + \frac{1}{\tau_{Aug}} + \frac{1}{\tau_{SRH}} + \frac{1}{\tau_{Surf}} = \frac{1}{\tau_{bulk}} + \frac{1}{\tau_{Surf}} \quad (2)$$

we can therefore obtain the emitter saturation current density J_{0e} of the symmetrically processed p⁺-n-p⁺ lifetime samples through assuming $J_{0\ front} = J_{0\ back} = J_{0e}$, which yields:

$$\begin{aligned} J_{0e} &= \frac{qn_i^2 W}{2} \frac{1}{N_d + \Delta n} \left(\frac{1}{\tau_{eff}} - \frac{1}{\tau_{bulk}} \right) \\ &= \frac{qn_i^2 W}{2} \frac{1}{N_d + \Delta n} \frac{1}{\tau_{Surf}} \end{aligned} \quad (3)$$

In the above equations, q is the fundamental charge, W is the wafer thickness, n_i is the intrinsic carrier concentration in silicon, N_d is the bulk doping concentration, Δn is the excess carrier concentration, τ_{bulk} is the bulk lifetime of the wafer, and τ_{Surf} is the lifetime of the associated with the surface recombination. Equation [3] presents the relationship between the J_{0e} and τ_{Surf} , where J_{0e} drops with τ_{Surf} increases. As we know, any impurities and dangling bonds at semiconductor surfaces promote the minority carrier recombination. The H-riched dielectrics (SiO₂, Al₂O₃, SiN_x:H, etc.) can amend these surface defects and unsaturated bonds (chemical passivation) and the Al₂O₃ with strong negative electric field can exclude minority carriers (electrons) of the p⁺ emitter surface (field effect passivation). Both of these two types of passivation can reduce the p⁺ emitter surface recombination to improve the lifetime τ_{Surf} and make the J_{0e} lower.

3.3. Performance analysis of bifacial solar cells with 2 and 4-nm Al₂O₃

In order to simplify the solar cell production process, we have not employed the Al₂O₃ postdeposition annealing procedure (350–450 °C, 10–30 min), because the industrial fast firing step (~800 °C peak firing temperature) could activate the surface passivation induced by Al₂O₃ [32]. We have successfully applied the thin (2 and 4 nm) Al₂O₃ passivated p⁺ emitter technology to the bifacial c-Si solar cells based on standard screen printed production lines under the conventional peak sintering temperature of 905 °C (30 s). It is noted that the following discussion is based on the thin (2 and 4 nm) Al₂O₃ passivated front side boron emitter of n-type bifacial c-Si solar cells. Figure 3 illustrates the distribution of the parameters V_{oc} , J_{sc} , FF , and Eff for the two groups' bifacial c-Si solar cells against the reference ones without Al₂O₃ passivation (0 nm). Apparently, the V_{oc} , J_{sc} , and Eff of the two groups exceed the reference group significantly. The average Eff reaches 20.25% for the bifacial c-Si solar cells, an absolute increase of 0.60% over the reference counterparts with an average Eff of 19.65%. The maximum Eff of 20.41% has been obtained on the bifacial c-Si solar cells with the 4 nm Al₂O₃

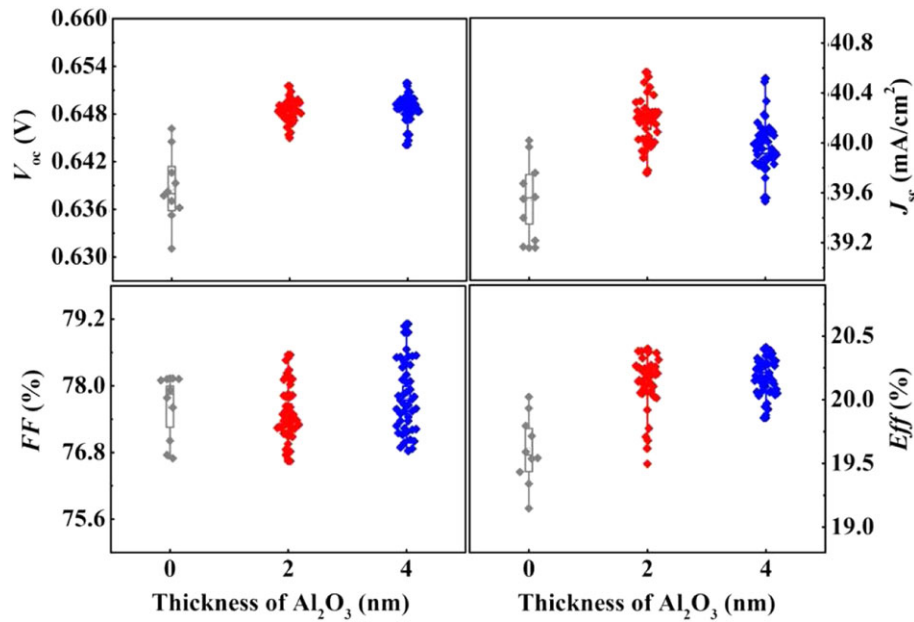


Figure 3. Electrical parameters (V_{oc} , J_{sc} , FF , and Eff) for the solar cells with two thin (2 and 4 nm) Al₂O₃ layers against the reference group without Al₂O₃ passivation (0 nm). [Colour figure can be viewed at wileyonlinelibrary.com]

dielectric passivation. Also, their average V_{oc} is more than 0.648 V, higher than that of the reference group with an average of 0.637 V. What is more, the convergence of all the electrical parameters on the 4 nm Al₂O₃ group is better than the other groups.

Richter *et al.* [33] have investigated the thermal stability and exact level of the Al₂O₃ passivation on the peak temperature and the duration of the sintering step. When Al₂O₃ surface passivation films are implemented in screen-printed solar cells, the thermal stability of the films during high-temperature firing processes (>800 °C) is crucial [12,34]. Figure 4 depicts the electrical parameters (V_{oc} , J_{sc} , FF , and Eff) of the screen-printed solar cells with the 2 and 4 nm Al₂O₃ associated with the different peak sintering temperatures from 895 to 920 °C. We have fabricated and measured 180 solar cells with each group of 30 pieces for six different peak sintering temperatures. The pillars and top error bars in the bar graphs of Figure 4 to represent the mean and maximum values of those electrical parameters, respectively. Here, we only adjust the peak sintering temperature at the conventional time of 30 s, in order not to change the sintering time of the other functional zones. Overall, the electrical parameters V_{oc} , FF , and Eff of the solar cells with the 4 nm Al₂O₃ group exceed those of the 2 nm Al₂O₃ counterpart. The best results of the electrical parameters (V_{oc} ~ 0.649 V, J_{sc} ~ 40.55 mA/cm², FF ~ 78.39% and Eff ~ 20.45%) are obtained simultaneously at the peak sintering temperature of 910 °C (30 s).

We further show in Figure 5 the EQE of the finished solar cells with the 2 and 4 nm Al₂O₃. It exhibits an appreciable difference in the short wavelength range from 300 to 420 nm but almost no change in the middle and long wavelength. This suggests that the observed improvement in the

cells with the 2 and 4 nm Al₂O₃ is associated with the emitter, rather than the bulk and BSF regions. In addition, the EQE trend in the short wavelength is consistent with the measured implied V_{oc} and τ_{eff} illustrated in Figure 2(b) and 2(c). These results clearly demonstrate that the significant improvement in the solar cells with thin Al₂O₃ layers comes from the enhancement in V_{oc} and J_{sc} , due to the improved passivation quality of the p⁺ emitters.

3.4. Influence of the screen printing technology on the solar cells performance

It should be noted from Figures 3 and 4 that the FF distribution of the two groups (2 and 4 nm Al₂O₃ passivation) is in the range from 76.64 to 78.96%, and most of the FF s are under 78%. This shows the detrimental impact of the screen-printed metallization contacts on the cell performance [35], and it is necessary to optimize the screen printing technology (e.g., fine lines and double printing (DP)) to match with the thin Al₂O₃ dielectric passivation process. As we all know, a narrow metal front side coverage results in decrease of shadowing and surface recombination but an increase of resistive losses [36]. The second printing with narrow fine fingers would compensate the resistive losses and lead to the excellent V_{oc} , J_{sc} , FF , and Eff [37]. In the present work, we have also employed the DP Ag/Al front side metallization technology featured a mesh-type screen with a four bus bars/85 fingers layer and 60 μm designed fingers aperture as a baseline or benchmark (We do not change the rear side standard single-printed Ag metallization design).

Figure 6 illustrates the electrical parameters (V_{oc} , J_{sc} , FF , and Eff) for the DP solar cells (333 pieces) with 4-

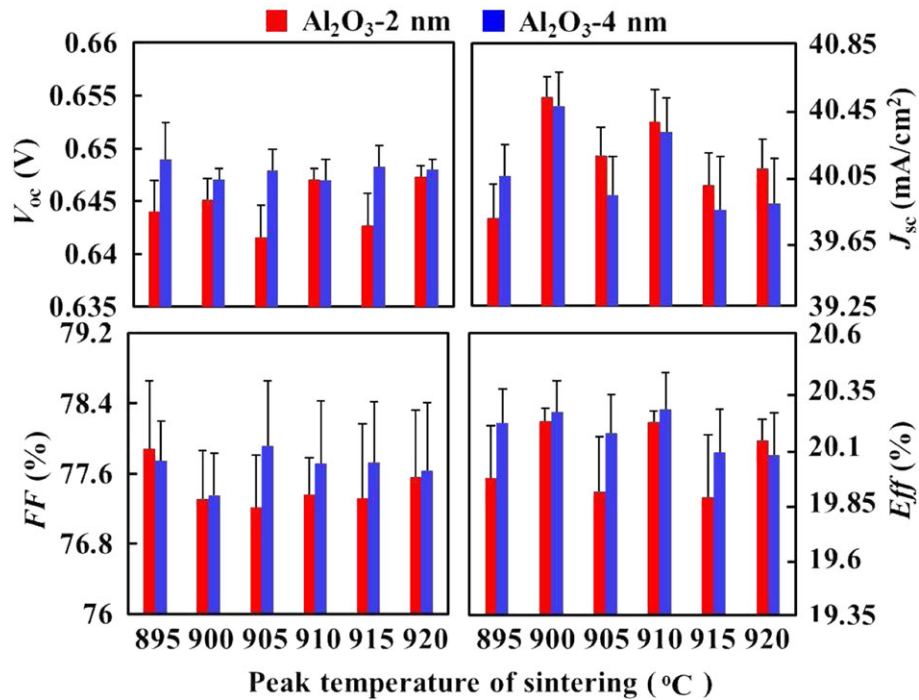


Figure 4. Electrical parameters (V_{oc} , J_{sc} , FF , and Eff) vary with the different peak temperatures of sintering. The pillars and top error bars in the bar graphs represent the mean and maximum values of those electrical parameters, respectively. [Colour figure can be viewed at wileyonlinelibrary.com]

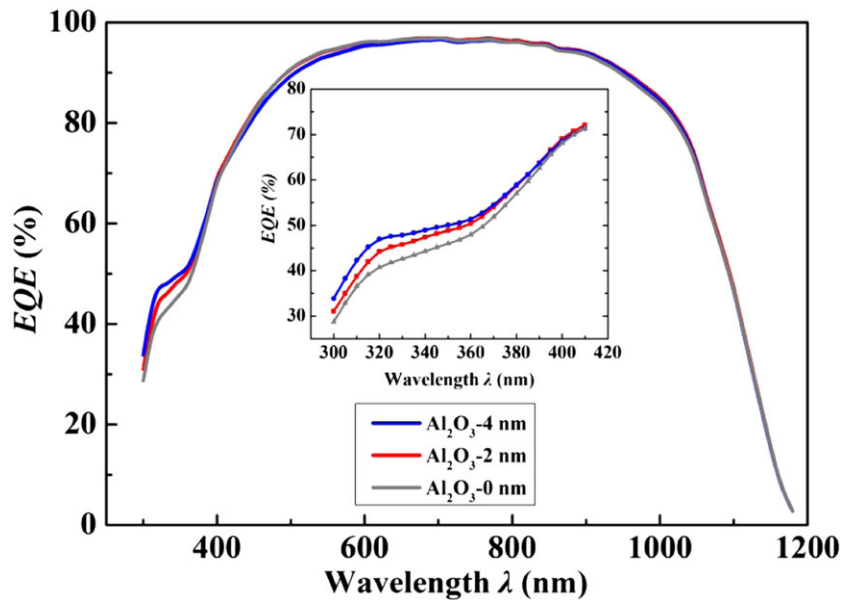


Figure 5. EQE as a function of the wavelength λ for the solar cells with two thin (2 and 4 nm) Al₂O₃ layers against the reference group without Al₂O₃ passivation (0 nm). [Colour figure can be viewed at wileyonlinelibrary.com]

nm Al₂O₃ passivated p⁺ emitter surfaces, including those with four different designed finer finger widths (48, 50, 52, and 55 μ m). Compared with the single-printed results shown in Figures 3 and 4, we can observe a clear increase

of average FF from 77.80% (single-printing) to 78.09% (60 μ m finger width DP baseline) and to 78.36% (50 μ m fine finger width DP). The average values of all the electrical parameters increase significantly with the V_{oc} of up

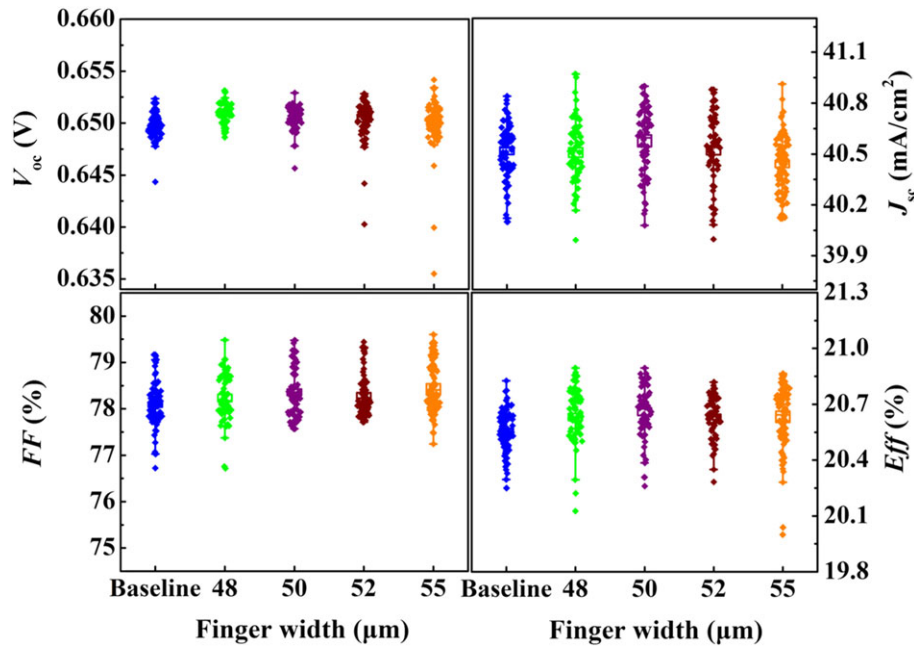


Figure 6. Electrical parameters (V_{oc} , J_{sc} , FF , and Eff) for the solar cells with 4 nm Al₂O₃ passivated p⁺ emitter surfaces under different designed fine finger widths and double printing technology at the peak sintering temperature of 910 °C (30 s). [Colour figure can be viewed at wileyonlinelibrary.com]

to 0.651 V, J_{sc} of 40.57 mA/cm², FF of 78.36% and Eff of 20.66% in the 50 μm fine finger width DP case. Too wide and too fine lines are not conducive to improve the performance of the solar cells. The wider the finger width is, the more serious the composite between metal and semiconductor is. The finer the finger width is, the easier the broken finger appears in the printing process. The maximum Eff of 20.89% has been achieved for the optimal front junction bifacial solar cell with 4 nm Al₂O₃ passivated p⁺ emitter surfaces and 50 μm fine finger width DP technology (Figure 7), and its back side cell Eff is 18.45%.

3.5. Optimization of n-type bifacial solar cells by PC1D simulation

We have employed PC1D software to calculate the conversion efficiency of the n-type bifacial Si solar cells varying with the different p⁺ emitter peak doping levels (from 9.38×10^{18} to 9.38×10^{20} cm⁻³) and bulk resistivities (1.5–5.5 Ω cm). Note that our experimental p⁺ emitter peak doping concentration is 9.38×10^{19} cm⁻³ (the sheet resistance R_{sh} is 63 Ω/□) and bulk resistivity is 3.5 Ω cm, where the calculated conversion efficiency Eff of 20.90% in Figure 8 is in good agreement with the experimental Eff of 20.89% in Figure 7. Figure 8 mainly concludes that the light doping concentration is beneficial to improve the conversion efficiency, with the maximum Eff up to 21.53% (at 1.5 Ω cm and 9.38×10^{18} cm⁻³ with the sheet resistance R_{sh} of 362.3 Ω/□). The advantage of the light doping concentration and high sheet resistance of the emitter come from the low Auger recombination

and excellent surface passivation [38]. As discussed in Figure 2(a), the indispensable annealing oxidation step not only activated the back side n⁺ BSF, but also decreased the front surface doping concentration with a higher sheet resistance and deeper junction depth of the p⁺ emitter. However, it is difficult to obtain low contact resistances when dealing with screen printed technology on high sheet-resistance emitters (>110 Ω/□) on a textured surface [39], where it is also not easy to reach good diffusion homogeneity all over the wafer surfaces along the boat in industrial high temperature diffusion process. As illustrated in Figure 8, an Eff of 21.32% can be achieved when we take a median doping concentration of 5.159×10^{19} cm⁻³ at 1.5 Ω cm with the sheet resistance R_{sh} of 103.9 Ω/□. Furthermore, Figure 8 also reveals that the Eff is not influenced obviously by the low bulk resistivity from 1.5 to 5.5 Ω cm under the fixed doping concentration.

3.6. Mass production feasibility of n-type bifacial Si solar cells

We have demonstrated a simple and feasible technology of thin Al₂O₃ (~4 nm) with SiN_x:H capped (~75 nm) films to effectively passivate the B-doped p⁺ emitter surfaces of the n-type bifacial c-Si solar cells with BBr₃ diffusion emitter and P ion-implanted BSF. The thin Al₂O₃ capped with SiN_x:H structure not only possesses the excellent field effect passivation and chemical passivation, but also establishes a simple cell structure and a low-cost manufacture process for cell efficiency over 20.8%. The investigated

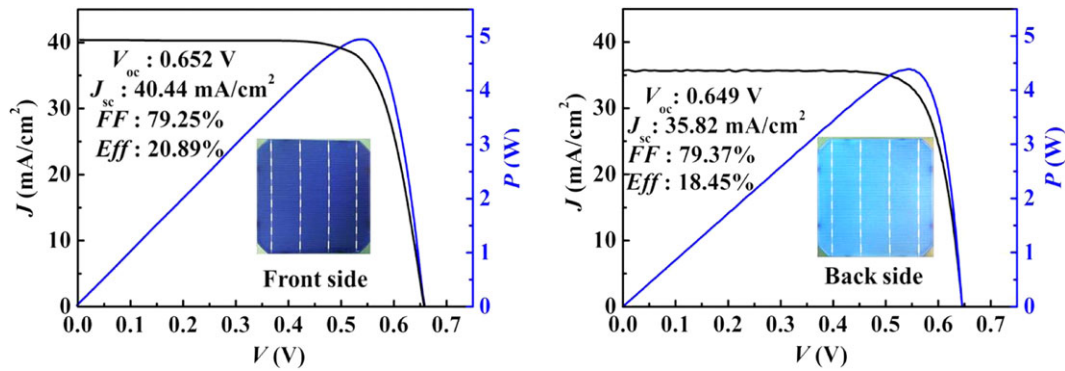


Figure 7. Output parameters, J - V , and power (P)- V characteristics for the optimal front junction bifacial solar cell with 4 nm Al₂O₃ passivated p⁺ emitter surface and 50 μ m fine finger widths double printing technology. The back side cell Eff is 18.45%. Shown in the inset is the photograph of the front and back side of the bifacial solar cell. [Colour figure can be viewed at wileyonlinelibrary.com]

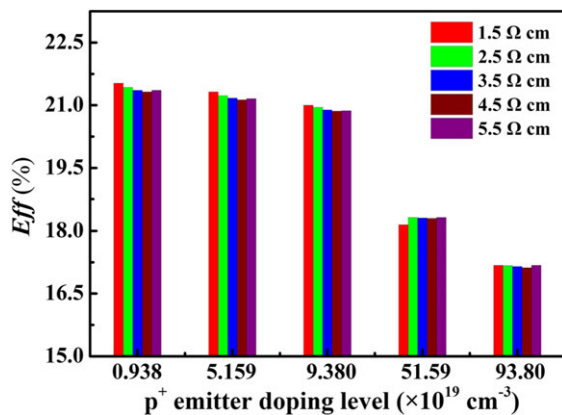


Figure 8. PC1D calculated n-type bifacial c-Si solar cell's conversion efficiency Eff versus p⁺ emitter doping level at different bulk resistivities (1.5–5.5 Ω cm). [Colour figure can be viewed at wileyonlinelibrary.com]

cell structure is fully compatible with the existing production lines and processes, i.e., there is no need to be annealed after the Al₂O₃ deposition procedure and to open the front side dielectric passivation layer with laser or etching pastes before the screen printing, as well as a simple co-firing step can be used for the two different metallization pastes (Ag/Al and Ag) to form electrical contacts for the front p⁺ emitter and n⁺ BSF, suitable for mass scale production. The present achievement can be further combined with the selective emitter technology for the high emitter sheet resistance of 100–110 Ω/\square , which decreases the recombination of the metal contact area of the p⁺ emitter surfaces and therefore improves the conversion efficiency Eff over 21.3%.

Finally, it should be noted that the present work focuses on the bifacial c-Si solar cells with industrial process, and currently, all the bifacial silicon solar cells are fabricated in conventional silicon production lines with the J - V measurements performed on the h.a.l.m. system. This test system does not exclude the reflected

lights from the rear side of the bifacial silicon solar cells; however, it is convenient and fast to assess the different classes of the bifacial solar cells in-line under different fabrication conditions, because the bifacial modules in real application operate under simultaneous front and rear side illumination (i.e., bifacial illumination). Moreover, there is no unified test standard on the bifacial solar cells in the world up to now. The present simplified cell structure and performance assessment have great advantages in the current low-cost n-type bifacial c-Si solar cell industrialization.

4. CONCLUSIONS

In summary, we have successfully achieved the large area (238.95 cm²) high efficiency of 20.89% (front) and 18.45% (rear) n-type bifacial c-Si solar cells using BBr₃ diffusion emitter and P ion-implanted BSF in conjunction with thin Al₂O₃ (4 nm) passivated p⁺ emitter technology. The passivation quality of the thin Al₂O₃ with SiN_x:H capped has been evaluated from the implied V_{oc} and τ_{eff} of the solar cell precursors, together with the theoretical simulation to understand the Al₂O₃/SiN_x:H stack passivation mechanism (chemical passivation and field effect passivation) of the p⁺ emitter surfaces. We have demonstrated that the performance of our n-type bifacial c-Si solar cells has been greatly enhanced by optimizing the peak sintering temperature and fine finger DP technology. We have further shown through the PC1D modeling that the conversion efficiency of our n-type bifacial Si solar cells can be improved to be over 21.3% by taking a lighter doping concentration with a higher emitter sheet resistance of 100–110 Ω/\square . The present simplified cell structure has great advantages in the low-cost n-type bifacial c-Si solar cell industrialization, not only effectively passivating the p⁺ emitter surfaces, but also fully compatible with the existing production lines and processes.

ACKNOWLEDGEMENTS

This work was supported by the Natural Science Foundation of China (61234005, 11674225 and 11474201), and Shanghai Municipal Project (14DZ1201000).

REFERENCES

- Macdonald D, Geerligs LJ. Recombination activity of interstitial iron and other transition metal point defects in p- and n-type crystalline silicon. *Applied Physics Letters* 2004; **85**(18): 4061–4063.
- Glunz SW, Rein S, Lee JY, Warta W. Minority carrier lifetime degradation in boron-doped Czochralski silicon. *Journal of Applied Physics* 2001; **90**(5): 2397–2404.
- Sepeai S, Zaidi SH, Desa MKM, Sulaiman MY, Ludin NA, Ibrahim MA, Sopian K. Design optimization of bifacial solar cell by PC1D simulation. *Journal of Energy Technologies and Policy* 2013; **3**(5): 1–11
- Romijn IG, Van Aken BB, Anker J, Barton P, Gutjahr A, Komatsu Y, Koppes M, Kossen EJ, Lamers M, Saynova DS, Tool CJJ, Zhang Y. Industrial cost effective n-Pasha solar cells with > 20% efficiency. In *Proceedings of the 28th European Photovoltaic Solar Energy Conference and Exhibition*. France: Paris, 2013. 736–40.
- Liu J, Janssen GJM, Koppes M, Kossen EJ, Tool K, Komatsu Y, Anker J, Gutjahr A, Vlooswijk A, Luchies JM, Siareyeva O, Granneman E, Romijn I. Selective emitter in n-type c-Si solar cells. In *Proceedings of the 31st European Photovoltaic Solar Energy Conference and Exhibition*. : Hamburg, Germany, 2015. 633–636.
- Agostinelli G, Delabie A, Vitanov P, Alexieva Z, Dekkers HFW, Wolf SD, Beaucarne G. Very low surface recombination velocities on p-type silicon wafers passivated with a dielectric with fixed negative charge. *Solar Energy Materials and Solar Cells* 2006; **90**(18): 3438–3443.
- Gatz S, Plagwitz H, Altermatt PP, Terheiden B, Brendel R. Thermally stable surface passivation by a-Si:H/SiN double layers for crystalline silicon solar cells. In *Proceedings 23rd European Photovoltaic Solar Energy Conference and Exhibition*. Valencia: Spain, 2008. 1033–1035.
- Benick J, Hoex B, Van de Sanden MCM, Kesseles WMM, Schultz O, Glunz SW. High efficiency n-type Si solar cells on Al₂O₃-passivated boron emitters. *Applied Physics Letters* 2008; **92**(25): 253504-1–253504-3.
- Schmidt J, Werner F, Veith B, Zielke D, Bock R, Tiba V, Poodt P, Roozeboom F, Li A, Cuevas A, Brendel R. Industrially relevant Al₂O₃ deposition techniques for the surface passivation of Si solar cells. In *Proceedings of the 25th European Photovoltaic Solar Energy Conference*. Valencia: Spain, 2010. 1130–1133.
- Dingemans G, Van de Sanden MCM, Kessels WMM. Influence of the deposition temperature on the c-Si surface passivation by Al₂O₃ films synthesized by ALD and PECVD. *Electrochemical and Solid-state Letters* 2010; **13**(3): H76–H79.
- Hoex B, Schmidt J, Bock R, Altermatt PP, van de Sanden MCM, Kessels WMM. Excellent passivation of highly doped p-type Si surfaces by the negative-charge-dielectric Al₂O₃. *Applied Physics Letters* 2007; **91**(11): 112107-1–112107-3.
- Dingemans G, Engelhart P, Seguin R, Einsele F, Hoex B, Van de Sanden MCM, Kessels WMM. Stability of Al₂O₃ and Al₂O₃/a-SiN_x:H stacks for surface passivation of crystalline silicon. *Journal of Applied Physics* 2009; **106**: 114907-1–114907-4.
- Dingemans G, Einsele F, Beyer W, Van de Sanden MCM, Kesseles WMM. Influence of annealing and Al₂O₃ properties on the hydrogen-induced passivation of the Si/SiO₂ interface. *Journal of Applied Physics* 2012; **111**(9): 093713-1–093713-9.
- Hoex B, Gielis JJH, Van de Sanden MCM, Kessels WMM. On the c-Si surface passivation mechanism by the negative-charge-dielectric Al₂O₃. *Journal of Applied Physics* 2008; **104**(11): 113703-1–113703-7
- Benick J, Richter A, Li T T A, Grant N E, McIntosh K R, Ren Y, Weber K J, Hermle M, Glunz S W. Effect of a post-deposition anneal on Al₂O₃/Si interface properties. In *35th IEEE Photovoltaic Specialists Conference (PVSC)*, 2010: 000891-000896.
- Liao B, Hoex B, Shetty KD, Bau PK, Bhatia CS. Passivation of boron-doped industrial silicon emitters by thermal atomic layer deposited titanium oxide. *IEEE Journal of Photovoltaics* 2015; **5**(4): 1062–1066
- Aboaf JA, Kerr DR, Bassous E. Charge in SiO₂-Al₂O₃ double layers on silicon. *Journal of the Electrochemical Society* 1973; **120**(8): 1103–1106.
- Johnson RS, Lucovsky G, Baumvol I. Physical and electrical properties of noncrystalline Al₂O₃ prepared by remote plasma enhanced chemical vapor deposition. *Journal of Vacuum Science & Technology A* 2001; **19**(4): 1353–1360.
- No SY, Eom D, Hwang CS, Kim HJ. Property changes of aluminum oxide thin films deposited by atomic layer deposition under photon radiation. *Journal of the Electrochemical Society* 2006; **153**(6): F87–F93.
- Werner F, Veith B, Zielke D, Kühnemund L, Tegenkamp C, Seibt M, Brendel R, Schmidt J. Electronic and chemical properties of the c-Si/Al₂O₃

- interface. *Journal of Applied Physics* 2011; **109**(11): 113701-1-113701-6.
21. Ok YW, Upadhyaya AD, Tao Y, Zimbardi F, Ryu K, Kang MH, Rohatgi A. Ion-implanted and screen-printed large area 20% efficient n-type front junction Si solar cells. *Solar Energy Materials and Solar Cells* 2014; **123**: 92-96.
 22. Müller R, Benick J, Bateman N, Schön J, Reichel C, Richter A, Hermle M, Glunz SW. Evaluation of implantation annealing for highly-doped selective boron emitters suitable for screen-printed contacts. *Solar Energy Materials and Solar Cells* 2014; **120**: 431-435.
 23. Cornagliotti E, Uruena A, Aleman M, Sharma A, Tous L, Russell R, Choulat P, Chen J, John J, Haslinger M, Duerinckx F, Dielissen B, Görtzen R, Black L, Szlufcik J. Large-area n-type PERT solar cells featuring rear p⁺ emitter passivated by ALD Al₂O₃. *IEEE Journal of Photovoltaics* 2015; **5**(5): 1366-1372.
 24. McIntosh KR, Altermatt PP, Ratcliff TJ, Fong KC, Black LE, Baker-Finch SC, Abbott MD. An examination of three common assumptions used to simulate recombination in heavily doped silicon. In *Proceedings of the 28th EU PVSEC*. France: Paris, 2013. 1672-1679.
 25. Altermatt PP, Schenk A, Schmihüsen B, Heiser G. A simulation model for the density of states and for incomplete ionization in crystalline silicon. II. Investigation of Si:As and Si:B and usage in device simulation. *Journal of Applied Physics* 2006; **100**: 113715-1-113715-7.
 26. Richter A, Glunz SW, Werner F, Schmidt J, Cuevas A. Improved quantitative description of Auger recombination in crystalline silicon. *Physical Review B* 2012; **86**(16): 165202-1-165202-14.
 27. Schenk A. Finite-temperature full random-phase approximation model of band gap narrowing for silicon device simulation. *Journal of Applied Physics* 1998; **84**(7): 3684-3695.
 28. Sinton RA, Cuevas A. Contactless determination of current-voltage characteristics and minority-carrier lifetimes in semiconductors from quasi-steady-state photoconductance data. *Applied Physics Letters* 1996; **69**(17): 2510-2512.
 29. Lee DY, Lee HH, Ahn JY, et al. A new back surface passivation stack for thin crystalline silicon solar cells with screen-printed back contacts. *Solar Energy Materials and Solar Cells* 2011; **95**(1): 26-29.
 30. Hofmann M, Kambor S, Schmidt C, Grambole D, Rentsch J, Glunz SW, Prue R. PECVD-ONO: a new deposited firing stable rear surface passivation layer system for crystalline silicon solar cells. *Advances in Optoelectronics* 2008; **2008**: 1-10.
 31. Aluminum oxide as negatively charged surface passivation for industrial crystalline silicon solar cells. n. [dhttps://www.researchgate.net/publication/234116427](https://www.researchgate.net/publication/234116427). [accessed 4 December 2016]
 32. Liao B, Stangl R, Ma F, Hameiri Z, Mueller T, Chi D, Aberla AG, Bhatia CS, Hoex B. Deposition temperature independent excellent passivation of highly boron doped silicon emitters by thermal atomic layer deposited Al₂O₃. *Journal of Applied Physics* 2013; **114**(9): 094505-1-094505-6.
 33. Richter A, Benick J, Hermle M. Boron emitter passivation with Al₂O₃ and Al₂O₃/SiN_x stacks using ALD Al₂O₃. *IEEE Journal of Photovoltaics* 2013; **3**(1): 236-245.
 34. Benick J, Richter A, Hermle M, Glunz SW. Thermal stability of the Al₂O₃ passivation on p-type silicon surfaces for solar cell applications. *Physica Status Solidi (RRL)-Rapid Research Letters* 2009; **3**(7,8): 233-235.
 35. Edler A, Mihailetchi VD, Koduvelikulathu LJ, Comparotto C, Kopecek R, Harney R. Metallization-induced recombination losses of bifacial silicon solar cells. *Progress in Photovoltaics: Research and Applications* 2015; **23**(5): 620-627.
 36. Dullweber T, Gatz S, Hannebauer H, Falcon T, Hesse R, Schmidt J, Brendel R. Towards 20% efficient large-area screen-printed rear-passivated silicon solar cells. *Progress in Photovoltaics: Research and Applications* 2012; **20**(6): 630-638.
 37. Kalio A, Richter A, Hörteis M, Glunz SW. Metallization of n-type silicon solar cells using fine line printing techniques. *Energy Procedia* 2011; **8**: 571-576.
 38. Zhong S, Shen W, Liu F, Li X. Mass production of high efficiency selective emitter crystalline silicon solar cells employing phosphorus ink technology. *Solar Energy Materials and Solar Cells* 2013; **117**: 483-488.
 39. Hörteis M, Glunz SW. Fine line printed silicon solar cells exceeding 20% efficiency. *Progress in Photovoltaics: Research and Applications* 2008; **16**(7): 555-560.